Journal of Controlled Release 237 (2016) 168–176

Contents lists available at ScienceDirect

Journal of Controlled Release

journal homepage: www.elsevier.com/locate/jconrel

Impact of surfactant treatment of paclitaxel nanocrystals on biodistribution and tumor accumulation in tumor-bearing mice

Wei Gao [a], Yan Chen [b], David H. Thompson [c], Kinam Park [a,d], Tonglei Li [a,*]

[a] Department of Industrial and Physical Pharmacy, Purdue University, West Lafayette, IN, United States
[b] Department of Pharmaceutics, School of Pharmacy, Second Military Medical University, Shanghai, China
[c] Department of Chemistry, Purdue University, West Lafayette, IN, United States
[d] School of Biomedical Engineering, Purdue University, West Lafayette, IN, United States

ARTICLE INFO

Article history:
Received 29 April 2016
Received in revised form 26 June 2016
Accepted 9 July 2016
Available online 11 July 2016

Keywords:
Paclitaxel
Nanocrystals
Biodistribution
PEG
Surfactant
Tumor

ABSTRACT

We have previously tested paclitaxel nanocrystals (PTX-NCs) in tumor murine models and learned that the nanocrystal formulation could achieve similar and superior anticancer efficacy to the conventional Taxol® formulation, but with significantly reduced side-effects. The nanocrystals were not coated with any surfactants and a majority of the injected dose was taken up by the liver (>40%), while a minimal amount was present in the blood circulation and quickly eliminated. The aim of this work was to treat the surface of PTX-NCs with PEG-based polymers and examine the impact by surface coating on biodistribution, pharmacokinetics, and tumor retention. Testing in tumor-bearing mice showed that PTX-NCs treated with Pluronic® F68 (PEG-PPG-PEG block polymer) significantly enhanced blood circulation of the drug and accumulation in tumor tissue. The absolute amount reaching the tumor, however, was still minimal relative to the dose.

1. Introduction

Nanocrystal (NC) formulation is a viable delivery platform, particularly for the cases of poorly soluble drugs [1–5]. Formulated into solid particles, drug NCs offer some unique advantages that traditional systems find difficult to match [6–8]. As the most stable physical state, crystals can maintain both the physical and chemical stability of the drug substance better than solubilized and/or encapsulated formulations. For nanocrystals that are produced directly by solution crystallization [9], surfactant use is generally minimal, thereby reducing possible toxic side-effects introduced by the surfactants. Drug loading can reach >90% even after surfactant coating. All these merits may lead to consistent and predictable biological performance.

Over the last few years, our laboratory was able to produce NCs of anticancer drugs via solution crystallization without the use of surfactants or excipients [10–15]. We subsequently examined the antitumor effects of the drug nanocrystals in murine xenograft models. Our results indicated that, compared with conventional solubilization/encapsulation formulations, the carrier-free nanocrystal system could achieve either similar or better antitumor efficacy with significantly reduced toxic effects [10,12]. Our biodistribution and pharmacokinetic data also showed that paclitaxel (PTX) NCs were rapidly cleared from blood circulation by the mononuclear phagocyte system (MPS), with >40% of injected dose found in the liver [12]. The enhanced permeability and retention (EPR) effect was limited in this case, accounting for <1% of the injected nanocrystals as tumor-associated. Since these nanocrystals were not surface-coated by any surfactants, they are expected to be hydrophobic, thereby contributing to the significant uptake by phagocytes in the liver of the PTX-NCs. It is, thus, interesting to evaluate whether surface modification of the drug nanocrystals, ideally by non-chemical means, could lead to reductions in liver uptake and increases in tumor accumulation.

PEGylation or surface treatment of a drug delivery system with PEG (polyethylene glycol) has been demonstrated to be effective in prolonging the circulation of many different delivery systems [16–21]. Various studies have illustrated that surface treatment enhances drug accumulation in tumor tissues when the EPR effect is prominent [22–24]. It is believed that the PEG polymer coating interacts preferentially with water molecules and forms a hydrophilic steric barrier that shields the delivery system from immediate recognition, opsonization, and elimination by the immune system [25,26].

The purpose of this study was to treat the surface of PTX-NCs with PEG-based surfactants and investigate its impact on the biodistribution and pharmacokinetics of the treated nanocrystals in mice. It was believed that the physical adsorption of the polymers could lower MPS uptake, prolong systemic circulation, and improve tumor accumulation. In the study, Pluronic® F68 was used as the surfactant for treating PTX-

* Corresponding author at: Department of Industrial and Physical Pharmacy, College of Pharmacy, Purdue University, Heine Pharmacy Building, 575 Stadium Mall Drive, West Lafayette, IN 47907, United States.
E-mail address: tonglei@purdue.edu (T. Li).

http://dx.doi.org/10.1016/j.jconrel.2016.07.015
0168-3659/

NCs. By doping nanocrystals with tritium-labeled PTX in the crystallization process, quantitative analyses of the drug concentration in the major organs and tumor of treated animals could be determined by scintillation counting. In addition, as described in our previous studies [12], a near-infrared (NIR) dye was physically integrated within the drug nanocrystals to enable full-body fluorescence imaging of live animals. Quantitative comparison of the biodistribution determined by scintillation and optical imaging was then performed. Significant improvement was seen in the biodistribution and pharmacokinetics of drug nanocrystals as a result of the surface treatment.

2. Materials and experimental procedures

2.1. Materials

Paclitaxel (>99.5% purity) was purchased from LC Laboratories (Woburn, MA, USA). Tritium-labeled paclitaxel (^{3}H-PTX, ≥97% chemical purity, 0.145 mCi/mL) was purchased from Moravek Biochemicals and Radiochemicals Co. (Brea, CA, USA). Indocyanine Green (maximum excitation wavelength, λ_{ex} = 760 nm; maximum emission, λ_{em} = 810 nm), Pluronic F68 and Cremophor EL® were obtained from Sigma-Aldrich Co. (St. Louis, MO, USA). Saline (0.9% w/v sodium chloride) for injection was obtained from Nerl Diagnostics Co. (Baltimore, MD, USA). Gibco® folate free RPMI-1640 medium and fetal bovine serum (FBS) were purchased from Life Technologies Co. (Grand Island, NY, USA). McCoy's 5A medium was provided by Corning Co. (Corning, NY, USA). Soluene® 350 was purchased from Perkin Elmer Inc. (Waltham, MA, USA). Ethanol was purchased from Decon Labs Inc. (King of Prussia, PA, USA).

2.2. Nanocrystal preparation

Paclitaxel pure nanocrystals (PTX-NCs) and paclitaxel hybrid nanocrystals integrated with indocyanine green (ICG) (PTX-ICG-NCs) were produced by the same anti-solvent method reported earlier [10,12]. Briefly, 1 mL of paclitaxel (3 mg/mL) ethanol solution was introduced to 20 mL deionized water in a 3-neck flask that was placed in a sonication water bath. The solution was then agitated with a stirrer shaft. Upon crystallization, the suspension was filtered through a 50-nm polycarbonate filter and the retentate was air dried prior to re-suspension in deionized water with a high-sheer homogenizer. The same procedure was used to produce hybrid nanocrystals, with the exception that ICG was dissolved in the deionized water prior to the introduction of the ethanol solution. Similarly, tritium-labeled nanocrystals were produced by adding 1 mL ethanol solution of 3 mg/mL (1.234 mCi/mol) of ^{3}H-paclitaxel to the crystallization medium.

To treat the nanocrystals with surfactant, 3 mg of PTX nanocrystals were re-suspended into 20 mL of 2% F68 solution for 10 min via bath sonication. The mixture was kept for 3 h at 4 °C, followed by triplicate centrifugation-washing-resuspension cycles in order to remove any loosely bound polymers.

Prior to each intravenous injection, the nanocrystals were suspended in saline at a concentration of 2 mg/mL. The Taxol formulation was prepared by dissolving the drug in a 50:50 mixture of ethanol and Cremophor EL® and adjusted with saline to 2 mg/mL.

2.3. Characteristics of PTX nanocrystals

2.3.1. Particle size and distribution

Particle size and size distribution of the nanocrystals were measured by dynamic light scattering (DLS) using a Malvern Zetasizer Nano ZS instrument (Zetasizer 3000HS, Malvern, Worcestershire, UK) at 25 °C. Each formulation was suitably diluted with saline to avoid multiple scattering. Each sample was measured in triplicate. DLS measures diffusion of suspended particles by detecting their Brownian motions. The particle size is then calculated from diffusion coefficient using Stokes-Einstein equation assuming spherical particle shape. It offers an estimate of particle size for non-spherical particles.

2.3.2. Morphology

Nanocrystals were examined using a scanning electron microscope (Nova Nano SEM, FEI, Hillsboro, OR, USA). Samples were dried under ambient conditions and then sputter-coated with gold palladium (Au/Pd) for 1 min prior to imaging.

2.3.3. Quantification of PTX and ^{3}H-PTX

An HPLC system (Agilent 1100, Agilent, Santa Clara, CA, USA) was used to determine the concentration of paclitaxel. The mobile phase consisted of acetonitrile and double-distilled water (50:50, *v*/v), with a flow rate of 1 mL/min. A UV detector was used and the absorption wavelength was set at 228 nm. An RP-18 column (4.6 mm × 150 mm, pore size 5 μm, Agilent Corporation, Philadelphia, PA, USA) was employed.

^{3}H levels in the radio-labeled nanocrystals were quantified with a liquid scintillation counter (Tri-Carb® 2900 TR Liquid Scintillation Analyzer, Packard BioScience Company, PerkinElmer Inc., Waltham, MA, USA). In general, a biological specimen (blood, tissue, or tumor) was first treated with 0.7 mL of Soluene 350. The sample was then held in a 50–60 °C oven until it was completely solubilized, yielding a yellowish solution. The sample was then cooled to room temperature and decolorized by mixing with 0.3 mL 30% hydrogen peroxide over 4 h. Hionic-Fluor scintillation cocktail (4 mL) was finally added to the sample and quenched in the dark for 1 h, prior to scintillation counting.

2.3.4. Polymer concentration in polymer-coated PTX nanocrystals

The F68 concentration in the polymer-coated nanocrystals was measured by an HPLC equipped with a charged aerosol detector (CAD). The chromatographic system consisted of an Agilent 1200 HPLC system (Agilent 1200, Agilent, Santa Clara, CA, USA) equipped with a pump, autosampler, temperature-controlled column compartment with a switching valve, and a Corona® CAD detector (ESA, Inc. Chelmsford, MA, USA). The analytical column used for separation was an Eclipse XDB-Phenyl column (2.1 mm × 150 mm, pore size 5 μm, Agilent Corporation, Philadelphia, PA, USA). The CAD settings were as follows: nebulizer temperature at 50 °C, and gas pressure between 3.3 and 3.6 bar. The mobile phase consisted of 0.1% acetic acid in water and 0.1% acetic acid in acetonitrile at a flow rate of 0.25 mL/min.

2.4. In vivo studies

Two human cancer cell lines, KB (nasopharyngeal epidermal carcinoma) and HT-29 (human colon adenocarcinoma), were obtained from American Type Culture Collection (ATCC) (Manassas, VA, USA). KB cells were cultured in folate free RPMI-1640 medium, while HT-29 cells were cultured in McCoy's 5A medium. Each medium was supplemented with 10% FBS and 1% penicillin streptomycin and cells were cultured at 37 °C in a humidified atmosphere containing 5% CO_2. The cells were passaged from T-flasks using 0.25% trypsin-EDTA after reaching approximately 90% confluence.

Female nude outbred mice (Tac:Cr:(NCr)-Foxn1 Nu) were obtained from Taconic Co. (Hudson, NY, USA) at 4–5 weeks of age (15–20 g) and kept under specific-pathogen-free condition for 1 week. before study. The animal experiment was approved by the Institutional Animal Care and Use Committee of Purdue University.

Table 1
Particle size and *Zeta* potentials of PTX-NCs.

Nanocrystals	Particle size (nm)	PDI	*Zeta* potentials (mV)
PTX-NCs	174 ± 13	0.27 ± 0.04	−14.8 ± 0.6
PTX/ICG-NCs	163 ± 13	0.20 ± 0.04	−27.3 ± 1.8
F68-PTX/ICG-NCs	187 ± 8	0.21 ± 0.02	−30.8 ± 0.6

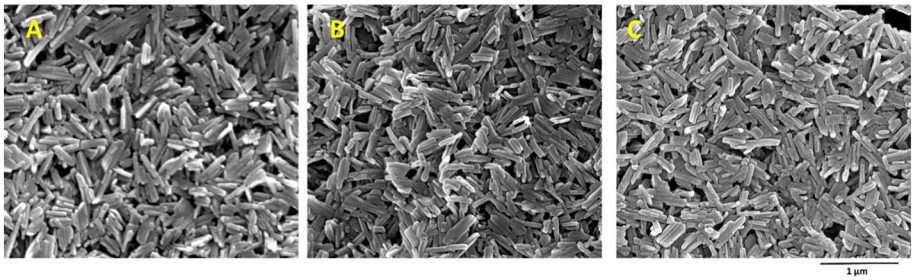

Fig. 1. SEM images of (A) PTX-NCs, (B) PTX-ICG-NCs hybrid nanocrystals, and (C) F68-PTX-ICG-NCs. Scale bar: 1 μm.

The tumor model in the study was established by subcutaneous injection of 3×10^6 HT-29 cells (100 μL) under the right arm and 3×10^6 KB cells (100 μL) under the left arm of nude mice. Tumors were allowed to grow for 9 d – average tumor size reached 200 mm^3 – before randomly dividing the mice into 4 treatment groups to minimize weight and tumor size variations among the groups (4 mice per group). The groups were treated with either Taxol, PTX-NCs, or F68-PTX-NCs at a dose of 20 mg/kg via tail vein injection. Individual body weights were monitored every day. Antitumor activity was evaluated in terms of tumor size (V), estimated by the following equation, $V = (L \times W^2) / 2$, where L is the longest and W is the shortest dimension of the tumor perpendicular to the length. After 7 days of treatment, the mice were sacrificed and the tumor tissues were removed and weighed.

To determine the biodistribution of F68-treated PTX-NCs, the animal preparation was conducted under the same protocol as described above. Tritium-labeled F68-PTX-ICG-NCs were administered intravenously once at a dose of 20 mg/kg via the tail vein injection. Each mouse received approximately 1 μCi of ^{3}H-PTX. At each predetermined time interval of 0.25, 0.5, 1, 2, 4, 6, 8, and 24 h, followed by 2, 3, 4, 5, 6, and 7 days, 4 mice were anesthetized with 3% isoflurane and imaged with an IVIS in vivo imaging system (Caliper IVIS Lumina II, PerkinElmer, Inc. Waltham, MA, USA). The excitation bandpass filter was set at 760 nm and emission was at 830 nm. Throughout the imaging process, 2% isoflurane delivery to an animal was maintained via a nose cone. All images were analyzed with IS2000MM software (Kodak, Rochester, NY, USA). Following the live imaging, mice were euthanized by CO_2 asphyxiation and cervical dislocation. Blood, tumors from both

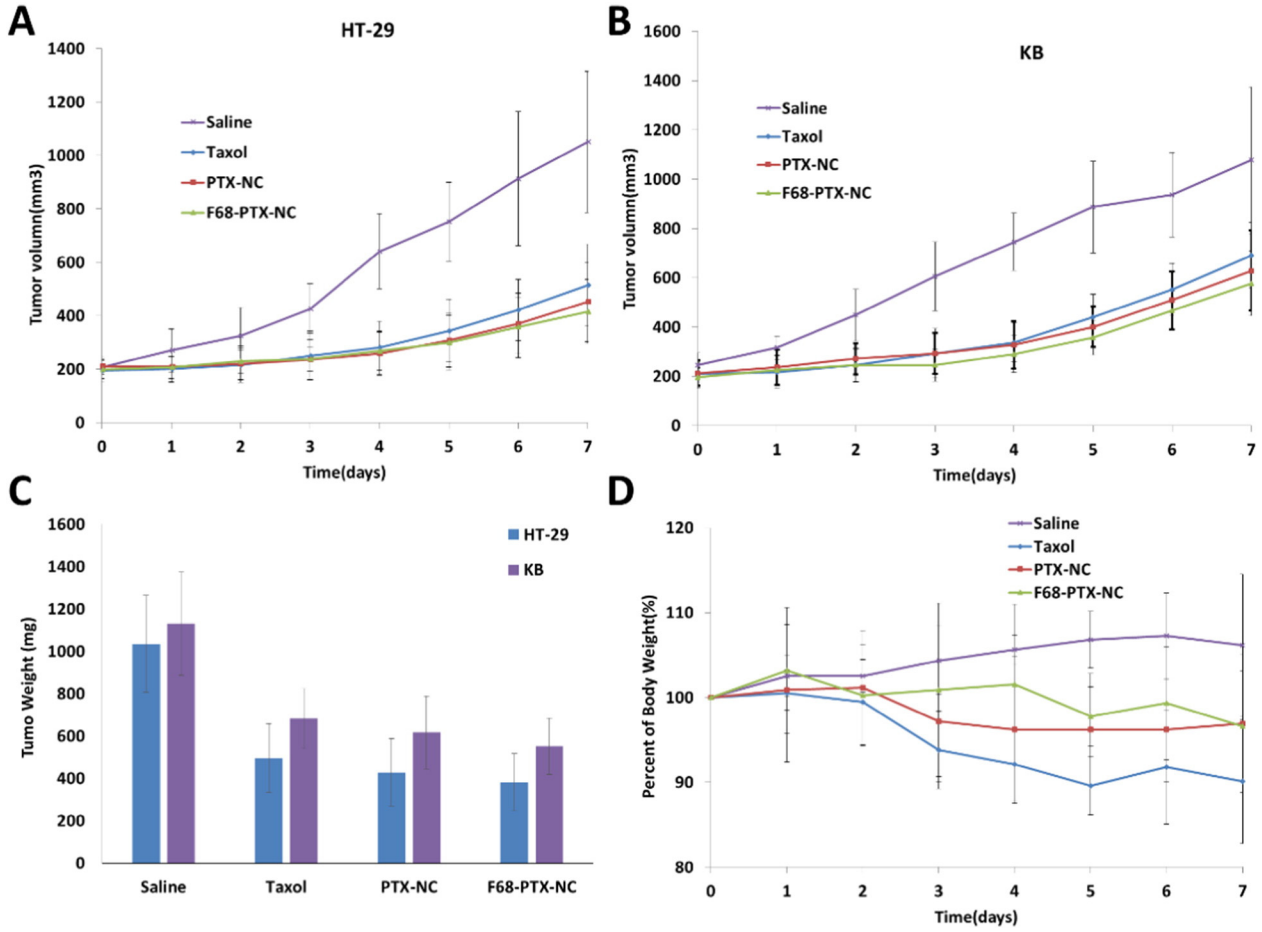

Fig. 2. Tumor volume progression of mice xenografted with (A) HT-29 cells and (B) KB cells treated with PTX-NCs, F68-PTX-NCs, Taxol, and saline, respectively. (C) Weights of excised tumors for each treatment group, measured at day 7. (D) Body weights of tumor-bearing mice was monitored for 7 days after drug injection. Each data point is presented as mean ± SD ($n = 4$). *$p < 0.05$.

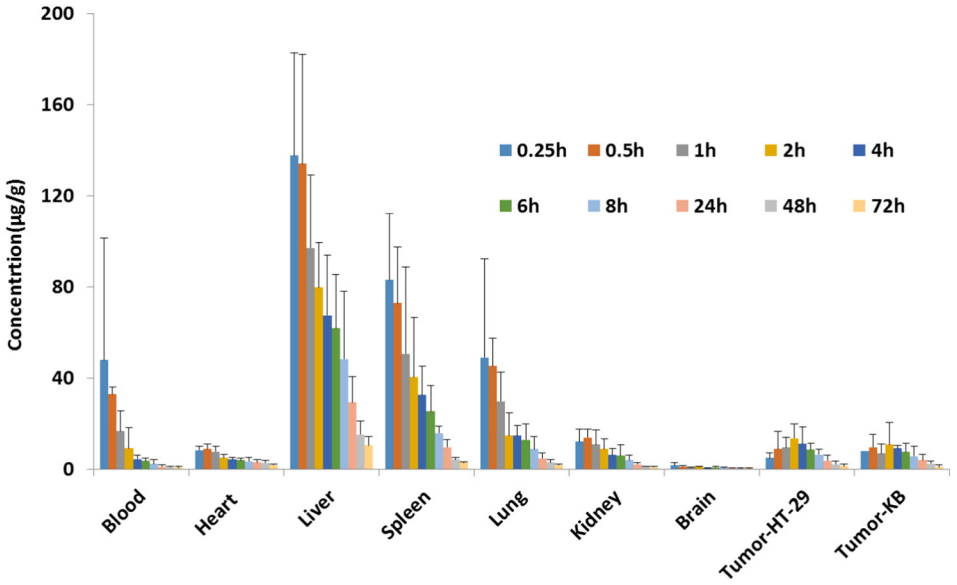

Fig. 3. Drug biodistribution of F68-^{3}H-PTX-ICG-NCs in the blood, tumors and major organs after intravenous administration at a dose of 20 mg/kg ($n = 4$). Each data point is normalized by the weight of the targeted organ.

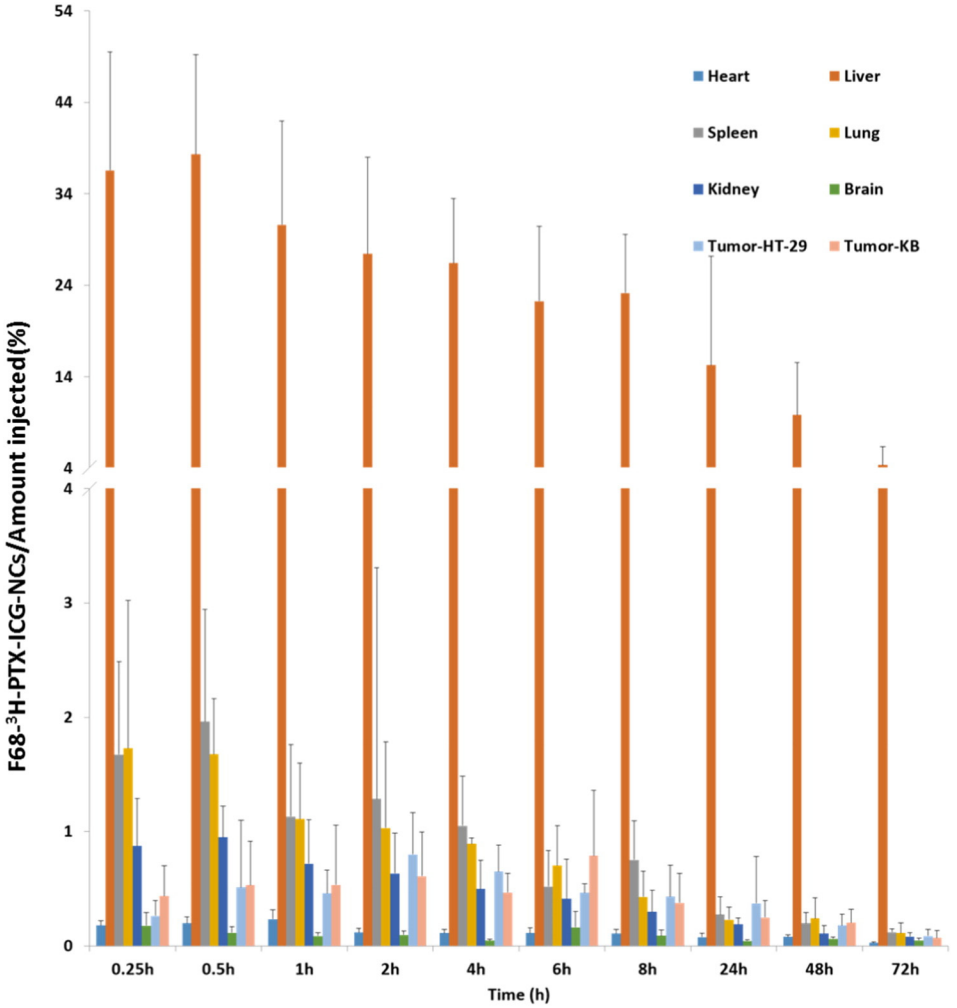

Fig. 4. Drug biodistribution of F68-^{3}H-PTX-ICG-NCs in the tumors and major organs as the percentage of the intravenously injected dose (20 mg/kg) ($n = 4$).

Table 2
Pharmacokinetic parameters of pure and F68-coated PTX nanocrystals. Each data is presented as mean ± standard deviation with $n = 4$.

	PTX-NCs	F68-PTX-NCs
C_{max} (μg/g)	3.0 ± 0.5	2.4 ± 1.3
$AUC_{(0\text{-}t)}$ (h × μg/g)	22.4 ± 19.0	48.2 ± 8.3
Cl_F (g/h/kg)	668.1 ± 553.1	137.3 ± 136.8
MRT (h)	22.4 ± 16.0	33.4 ± 2.0

sides of the flank, and major organs were excised from the animals, washed with cold saline, dried on filter paper, weighed, and imaged with IVIS. The samples were stored at −70 °C until scintillation analyses.

2.5. Pharmacokinetics calculation and statistical analysis

Non-compartmental pharmacokinetic analysis (NCA) was used to analyze in vivo drug plasma concentrations at various time points with Phoenix 64 (Pharsight Corporation, Palo Alto, CA, USA). The program was used to analyze pharmacokinetics parameters including the maximum plasma drug concentration (C_{max}), the area under the plasma concentration time curve (AUC), total body clearance (CL), and the mean residence time (MRT) of PTX nanocrystals.

All data is presented as mean ± standard deviation (SD) of independent measurements unless stated otherwise. Student's *t*-test or one-way analysis of variance (ANOVA) was performed for significance evaluation. A *p*-value of <0.05 was considered to be statistically significant and <0.01 was considered to be of high significance.

3. Results and discussion

3.1. Nanocrystal characterization

The average particle size of PTX pure and hybrid nanocrystals, determined by DLS (Table 1), was 174 ± 13 nm for PTX-NCs. Physical integration of ICG into the crystals (PTX-ICG-NCs) produced slightly smaller particles (163 ± 13 nm), whose ICG content in the nanocrystals was found to be 3.38 ± 0.26% before coating the PTX-NCs with F68. After F68 coating, the particle size increased to 187 ± 8 nm. However, the particle size changes are not statistically significantly. Because of safety concerns, the radio-labeled nanocrystals for treating the animals were not washed and centrifuged after being incubated with F68. Accordingly, using non-radio-labeled nanocrystals to estimate the surfactant concentration, it was found that the F68 content in the F68-PTX-NCs measured by HPLC-CAD was 20.1 ± 2.2% by weight (i.e., the ratio of F68 mass to the sum of the F68 and paclitaxel masses). However, when F68-PTX-NCs were washed, centrifuged, and re-suspended for three times, the polymer content was 4.97 ± 0.5%. As such, it is likely that the actual amount of F68 that was tightly bound to the nanocrystals for the animal studies could be much lower than the experimentally measured value. All three samples had small PDI values around 0.2, indicating narrow size distributions. The nanocrystals exhibited well-defined, rod-like morphologies with a long axis of approximately 200 nm in average by SEM (Fig. 1), as reported previously [12]. Radio-labeled nanocrystals were not measured or imaged due to safety concerns; however, they were expected to have similar sizes and morphologies as shown in Fig. 1 since the same crystallization methods were used for their production.

3.2. Antitumor efficacy

To investigate the antitumor effects of the drug nanocrystals, tumor-bearing mice were treated with either PTX-NCs or F68-PTX-NCs, using Taxol and saline as control groups. Each animal was implanted with HT-29 and KB cells, respectively, on opposing flank areas. Tumor volumes as a function of time were monitored and the results are shown in Fig. 2. Tumor volumes of HT-29 treated with either PTX-NCs or F68-PTX-NCs were consistently smaller than those observed with Taxol treatment throughout the whole observation period, with the F68-PTX-NCs exhibiting slightly higher efficacy than untreated PTX-NCs toward tumor growth inhibition. Nonetheless, the efficacy difference between the treatment types was statistically insignificant among the groups. During the first four days after drug injection, tumor growth suppression was almost complete for all three treatment groups. Tumors started to re-grow after 4 days, with growth rates observed to be faster in the Taxol group than the other two groups. We attribute these observations to rapid drug elimination after the single injection of the Taxol formulation. These results also suggest that the nanocrystal PTX dispersions produce longer half times in tumor tissue, as previously observed [12]. Similar trends in antitumor efficacy were observed in KB tumor volume experiments (Fig. 2B). Tumors that were treated with either PTX-NCs or F68-PTX-NCs were smaller in volume and mass than those by Taxol (Fig. 2B and C). Our results also showed that HT-29 tumors were more sensitive to PTX treatment than KB tumors.

Body weight of the animals was monitored as a general measure of treatment toxicity (Fig. 2D). Weight loss was generally lower for the nanocrystal-treated groups than for the Taxol-treated mice. Body

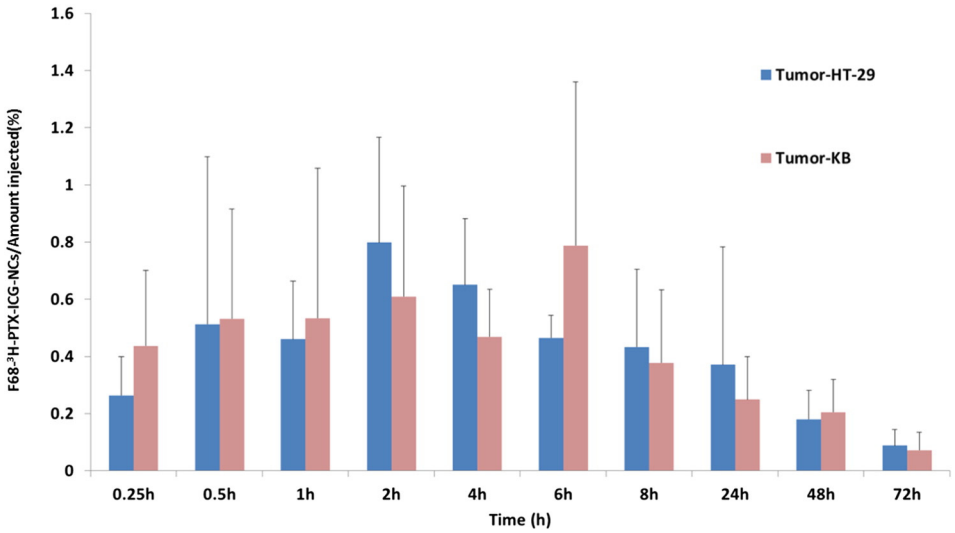

Fig. 5. Drug percentage of intravenously injected F68-^{3}H-PTX-ICG-NCs (20 mg/kg) in KB and HT-29 tumors as the percentage ($n = 4$).

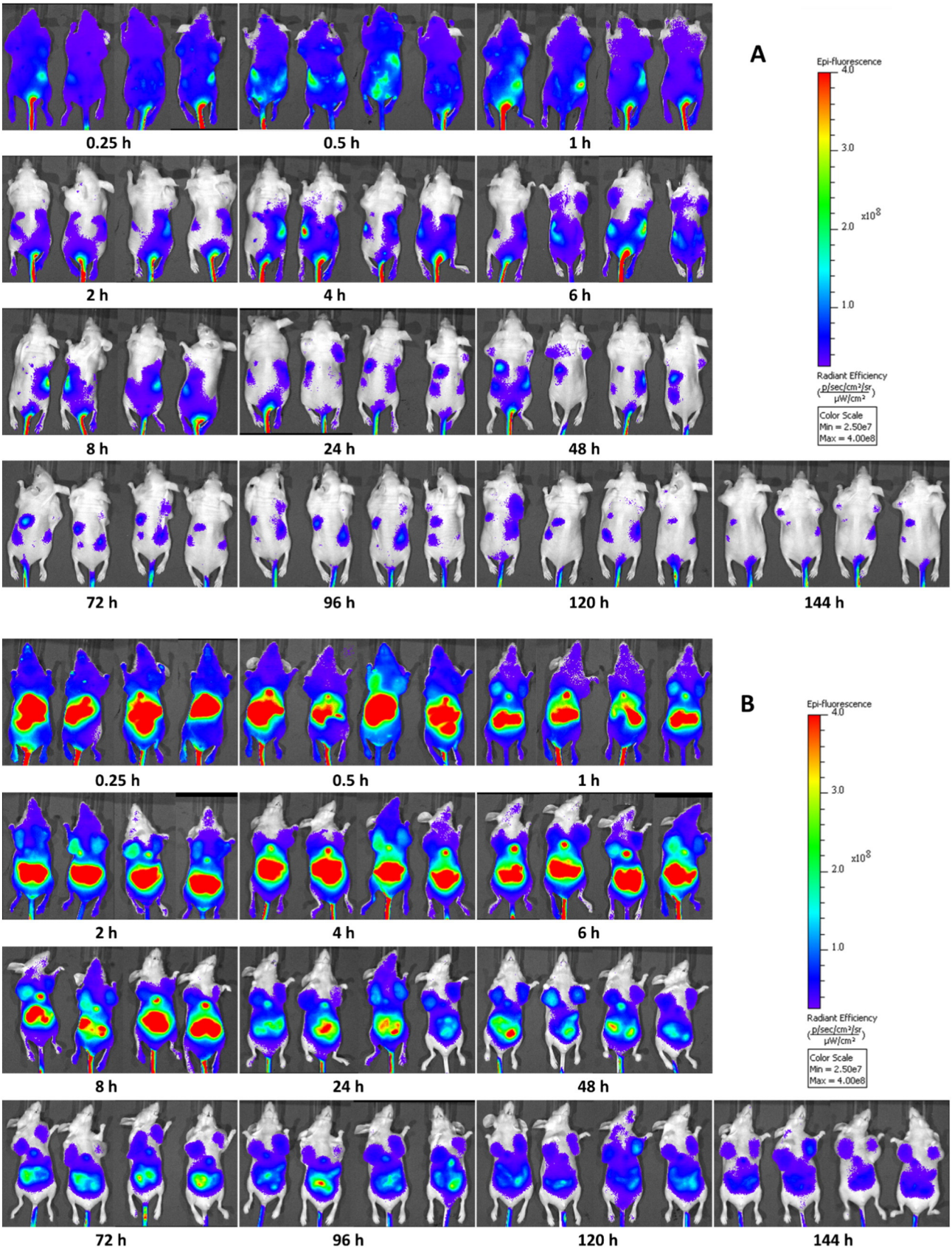

Fig. 6. In vivo imaging of HT-29 and KB tumor-bearing mice after i.v. injection of F68-^{3}H-PTX-ICG-NCs from (A) dorsal and (B) ventral views.

weight loss was 3.0 ± 8.2% and 3.3 ± 6.5% on day 7, for mice treated with PTX-NCs and F68-PTX-NCs, respectively; whereas body weights of the Taxol treated group were reduced significantly, reaching 9.9 ± 7.3% on day 7. Between the two nanocrystal treatment groups, the F68-cotated formulation seemed to be better tolerated as there was no significant reduction in body weight until day 5. These results show that the nanocrystal formulations exhibited less systemic toxicity than Taxol, which is known to cause hypersensitivity reactions and cardiotoxicity due to its solubilizing agent, Cremophor EL [27–29]. Overall, our results indicate that the F68-PTX-NCs and PTX-NCs exert comparable or better therapeutic efficacies with less systemic toxicity than the conventional PTX formulation.

3.3. Biodistribution of drug nanocrystals

Our previous study indicated that a large portion of pure PTX-NCs were taken up by the liver immediately after the formulation was administered intravenously to tumor-bearing mice [12]. This study was intended to evaluate the impact of PEG-based surfactant-coated drug nanocrystals on the biodistribution of PTX-NCs. Tritium-labeled F68-PTX-NCs (F68-^{3}H-PTX-ICG-NCs) were administered by tail vein injection into nude mice that were implanted subcutaneously on opposing flanks with HT-29 and KB tumors. Note that, due to radiation safety concerns, the polymer-coated ^{3}H-PTX nanocrystals were not subjected to washing-centrifugation-reconstitution cycles and used directly in the animals. The drug concentration in the blood, heart, liver, spleen, lungs, kidneys, and tumors that were collected from euthanized animals was measured by scintillation counting at predetermined time points (Figs. 3 and 4). Within 15 min of administration, the drug was detected in the major organs.

Compared with our previous results [12], the impact by the polymer treatment was substantial. First, the drug concentration increased significantly in blood circulation. The blood concentrations of drug 15 min after Taxol and PTX-NCs administration were 12.14 ± 1.01 and 1.76 ± 2.08 μg/g [12], respectively, while the concentration reached 47.83 ± 53.64 μg/g at the same time point when F68-PTX-NCs were administered. F68 coating of the PTX-NCs led to the increase in blood concentration by 27 and 4 times, respectively, compared with using pure drug nanocrystals and Taxol. Interestingly, the enhancement showed different blood elimination trends. Relative to pure PTX-NCs, F68-PTX-NCs yielded higher blood drug concentrations 23.0, 22.5, 8.6, 5.3 and 2.2 times at 0.25, 0.5, 1, 8 and 24 h, respectively. Increased drug retention by F68-PTX-NCs relative to Taxol was also demonstrated by concentration ratios of 3.9, 4.2, 4.0, 8.5 and 6.7 at the same time points, clearly showing that the nanocrystals were eliminated more slowly from blood circulation than Taxol.

We thereby infer from these findings that PTX-NCs surface modification with F68 yielded a significant blood circulation enhancement. Without the PEG-based polymers, the highly hydrophobic surface of the nanocrystals is expected to significantly promote adhesion of complement proteins in the plasma [30]. In contrast, the adsorption of hydrophilic chains onto the crystal surface can lead to a reduction in protein binding and subsequent recognition by RES [31–34]. It is expected that the hydrodynamic processes in blood circulation can significantly peel off adsorbed F68, especially those loosely bound to the surface. A small proportion of those tightly bound could still produce a significant enhancement in the blood circulation of the polymer-coated nanocrystals. Of the total dose injected intravenously, about 15.87 ± 11.82% was measured at the first data point (15 min) in the blood, compared with 0.42 ± 0.12% of untreated nanocrystals and 2.89 ± 0.24% of Taxol reported previously [12].

Table 2 shows the comparison of pharmacokinetic (PK) properties determined of PTX nanocrystals. Of pure PTX NCs, data was taken from our previous study results [12]. Of both in vivo experiments to evaluate the pure and F68-coated nanocrystals, there were four animals that were examined at each time point. From the PK results, it is apparent that F68-PTX-NCs achieved a larger AUC (>2 folds) and a longer retention time (>1.4 folds), whilst PTX-NCs were more quickly eliminated from circulation. Based on the clearance of pure and F68-coated PTX nanocrystals, which were 668.1 ± 553.1 g/h/kg vs. 137.3 ± 136.8 g/h/kg, respectively, there was 5 times more of plasma being cleared of pure PTX nanocrystals than coated nanocrystals within the same time period.

The biodistribution data further indicates that the nanocrystals were taken up primarily by the liver, followed by the spleen and lungs (Fig. 3). The data is plotted as the normalized amount of drug in an organ (μg/g). When the drug amounts are plotted out of the injected dose, close to 40% of the polymer-coated nanocrystals were taken up by the liver (Fig. 4), down a few percent compared with untreated nanocrystals [12]. The highest levels of liver deposition by F68-^{3}H-PTX-ICG-NCs was about 38%, compared with 42% for pure PTX-NCs. The polymer treatment of the nanocrystals modestly reduced liver sequestration by the MPS, likely due to their reduced hydrophobicity and steric shell by polymer chains. Drug elimination from the liver also occurred more rapidly for the F68-^{3}H-PTX-ICG-NCs formulation than for the untreated nanocrystals [12]. Similar tissue distributions were observed in other organs for the polymer-treated and pure nanocrystal dispersions. No more than 2% of the injected dose of F68-^{3}H-PTX-ICG-NCs or pure PTX-NCs were taken up by the spleen and lungs, respectively, which

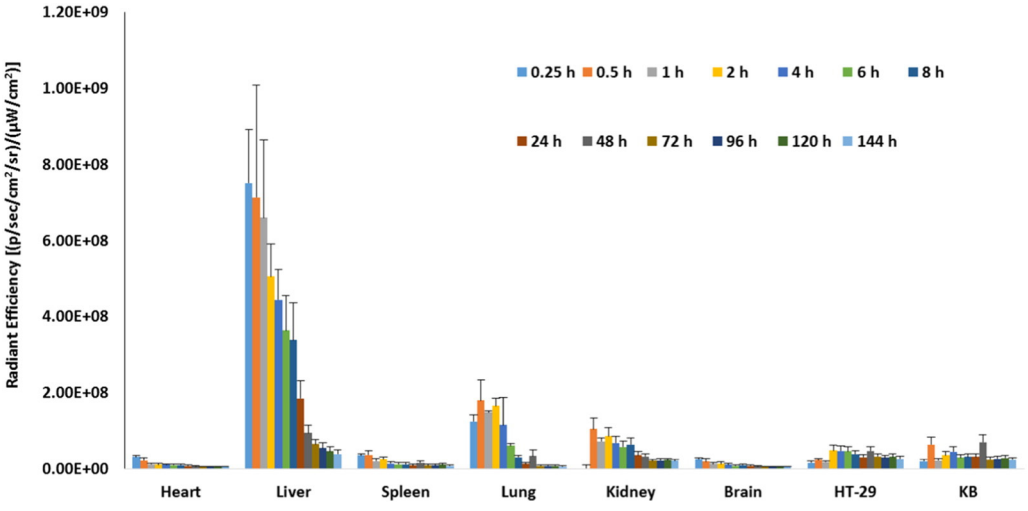

Fig. 7. Analysis of mean fluorescence signal in tumor and organs. The results are presented as the mean ± SD ($n = 4$).

was higher than Taxol. Less than 1% of the injected dose of F68-^{3}H-PTX-ICG-NCs or pure PTX-NCs were found in the kidneys, lower than that by Taxol which was about 1.25% at the first data point (15 min).

Moreover, the biodistribution results suggest that the tumor uptake of F68-^{3}H-PTX-ICG-NCs showed a graduate increase within the first a few hours of administration (Fig. 5), with a peak drug concentration of about 0.8% in the HT-29 (at 2 h) and 0.8% in KB (at 6 h), followed by a steady decrease in tumor-associated drug concentration. The kinetic behavior in the tumor differs from the trend observed in the other organs and blood, which reached the maximal concentration by 15 min and monotonically diminished afterwards. The prolonged blood circulation of polymer-coated nanocrystals contributed to the tumor accumulation, alone with the liver-captured nanocrystals potentially behaving as "depots" that continued to release the drug back to the systemic circulation leading to the increased drug concentration in the tumor. We hypothesize that some drug nanocrystals were retained in the tumor and prevented from returning to the blood and/or lymphatic circulation due to their size (approximately 200 nm) and elongated morphology. The total drug accumulation to both tumor sites reached almost 2%, more than 3 times the concentration by using pure drug nanocrystals observed in our previous study (in which only HT-29 tumors grew on the both sides of flank) [12]. Since there was little difference in tumor accumulation between KB and HT-29 tumors in this study (Fig. 5), we can attribute the significantly increased drug concentration to the polymer coating on the nanocrystals. Still, the proportion of the total injected dose reaching the tumor was a few percent at maximum, consistent with our earlier findings that the EPR effect may be limited in this animal model [12]. The weight-normalized biodistribution data (Fig. 3) suggests that drug uptake in the tumor was similar to that in the spleen, but far smaller than the levels found in liver, lungs, or kidneys. The liver generally weighs 4–5 times heavier than the tumor, but it took up 30–40 times more drug in comparison. We primarily attribute this difference to the blood flows (rate and volume) in each tissue type, which is largely determined by the vascular density and organization. The poorly developed blood vessels of tumor tissue, along with high interstitial fluid pressure, may actually limit drug uptake, with EPR and clearance playing a secondary role. The primary conclusion of this aspect of the study is that the polymer coating on the nanocrystals promoted a significant increase in tumor accumulation, likely due to the prolonged blood circulation of the drug delivery system.

3.4. Whole-body bioimaging

The nanocrystals used in the biodistribution study also contained an NIR dye, ICG, which was physically integrated inside the drug crystals. Whole-body bioimaging of live animals was then conducted to gain additional understanding of the drug distribution after nanocrystal administration. Mice that were treated with F68-^{3}H-PTX-ICG-NCs were imaged from the dorsal and ventral sides at pre-determined time points (Fig. 6). ICG fluorescence was monitored throughout the animal within 15 min of i.v. administration. Rapid distribution of fluorescence signals throughout an animal is attributed to the nanocrystal distribution kinetics, because their complete dissolution is unlikely at this timescale. Note that in vivo dissolution kinetics of the drug nanocrystals is difficult to determine, but their complete dissolution under sink conditions in vitro may take several dozens of minutes (unpublished results). From the ventral side images, the fluorescent intensity in the liver area was the highest throughout the experiment, consistent with the drug biodistribution results as determined by scintillation counting (Figs. 3 and 4). Fluorescence appeared in the tumors after 1 h and became gradually intensified within 1 day. After 24 h, the optical intensities started to fade. The intensity decrease of the tumor was relatively slower than those in other areas. This seems to be in agreement with the slow clearance of the drug from tumor sites (Fig. 5). Moreover, the fluorescence of the HT-29 tumor (under the right arm) was initially stronger than that of the KB tumor (under the left arm); however, at later stages of the experiment, the intensities of the KB tumor became stronger. These findings are consistent with the tumor accumulation data shown in Fig. 5.

3.5. Ex vivo imaging

Upon euthanization of the animals used in the whole-body imaging, tumors and major organs were excised for both ex vivo fluorescence imaging and scintillation counting. The tissue samples were homogenized and fluorescent intensities were quantitatively integrated over the processed samples. The results, shown in Fig. 7, indicate that the liver bore the highest intensities at all of the time points. The ICG fluorescence intensities in the lungs and kidneys were much higher than would be suggested by the drug biodistribution results (Fig. 3). The fluorescence intensities decreased rapidly in the heart, liver, lungs, spleen, and kidneys, with the tumor-associated intensities gradually increasing and steadily maintained after 8 h. Compared with the drug biodistribution results (Figs. 3 and 4), the bioimaging data overestimated the biodistribution in the tumors and produced large discrepancies in the observed tissue association in lungs and kidneys. Similar observations were made in our previous study of PTX nanocrystals without polymer coating [12]. It should be noted that the bioimaging results reflect the distribution of the NIR dye, ICG, not the drug. ICG alone can be cleared rapidly with a half-life of 2–4 min in plasma [35–37]. Still, the results at initial time points may represent the biodistribution of drug nanocrystals because the dye was mostly integrated within the nanocrystals. As the nanocrystals started to dissolve, the dye molecules could undergo different distribution routes and fates from those of the nanocrystals or dissolved drug molecules. The bioimaging results may thus be used for estimating the drug distribution in a semi-quantitative fashion.

4. Conclusion

This study examined the influence of physical adsorption of PEG-based surfactants on PTX nanocrystals and the impact this polymer coating may have on antitumor efficacy and nanocrystal biodistribution. The nanocrystals demonstrated equal or better treatment efficacy and less toxicity than Taxol in tumor murine models. Significantly prolonged blood circulation was observed, compared with untreated drug nanocrystals. Liver uptake of the polymer-treated nanocrystals remained significant and comparable, along with other organs, relative to the uptake of untreated nanocrystals. Tumor accumulation of the drug became enhanced by three or four times, most likely due to the prolonged blood circulation. The absolute amount of drug within the tumor was nonetheless minor, likely due to poorly developed vasculature and subsequently limited blood flow. In addition, the hybrid nanocrystals permitted whole-body bioimaging. Ex vivo imaging results of the tumors and organs agree with the drug biodistribution semi-quantitatively. Overall, this study demonstrated the feasibility and treatment benefit of using polymeric surfactants to coat drug nanocrystals. The impact on treatment efficacy and drug biodistribution was positive.

Acknowledgements

This work was financially supported by Lilly Endowment Seed Grant Program and Chao Endowment. We also thank Dr. Xingang Li from Department of Pharmacy, Beijing Tiantan Hospital, China, for assistance with PK analyses.

References

[1] E. Merisko-Liversidge, P. Sarpotdar, J. Bruno, S. Hajj, L. Wei, N. Peltier, J. Rake, J.M. Shaw, S. Pugh, L. Polin, J. Jones, T. Corbett, E. Cooper, G.G. Liversidge, Formulation and antitumor activity evaluation of nanocrystalline suspensions of poorly soluble anticancer drugs, Pharm. Res. 13 (1996) 272–278.

[2] B.E. Rabinow, Nanosuspensions in drug delivery, Nat. Rev. Drug Discov. 3 (2004) 785–796.
[3] H.K. Chan, P.C.L. Kwok, Production methods for nanodrug particles using the bottom-up approach, Adv. Drug Deliv. Rev. 63 (2011) 406–416.
[4] R.H. Muller, C. Jacobs, O. Kayser, Nanosuspensions as particulate drug formulations in therapy rationale for development and what we can expect for the future, Adv. Drug Deliv. Rev. 47 (2001) 3–19.
[5] R. Shegokar, R.H. Muller, Nanocrystals: industrially feasible multifunctional formulation technology for poorly soluble actives, Int. J. Pharm. 399 (2010) 129–139.
[6] E. Merisko-Liversidge, G.G. Liversidge, E.R. Cooper, Nanocrystal drug particles: resolving pharmaceutical formulation issues associated with poorly water-soluble compounds, Abstr. Pap. Am. Chem. Soc. 226 (2003) U528.
[7] F. Liu, J.Y. Park, Y. Zhang, C. Conwell, Y. Liu, S.R. Bathula, L. Huang, Targeted cancer therapy with novel high drug-loading nanocrystals, J. Pharm. Sci. 99 (2010) 3542–3551.
[8] E. Merisko-Liversidge, G.G. Liversidge, E.R. Cooper, Nanosizing: a formulation approach for poorly-water-soluble compounds, Eur. J. Pharm. Sci. 18 (2003) 113–120.
[9] E.M. Merisko-Liversidge, G.G. Liversidge, Drug nanoparticles: formulating poorly water-soluble compounds, Toxicol. Pathol. 36 (2008) 43–48.
[10] R.S. Zhao, C.P. Hollis, H. Zhang, L.L. Sun, R.A. Gemeinhart, T.L. Li, Hybrid nanocrystals: achieving concurrent therapeutic and bioimaging functionalities toward solid tumors, Mol. Pharm. 8 (2011) 1985–1991.
[11] H. Zhang, C.P. Hollis, Q. Zhang, T.L. Li, Preparation and antitumor study of camptothecin nanocrystals, Int. J. Pharm. 415 (2011) 293–300.
[12] C.P. Hollis, H.L. Weiss, M. Leggas, B.M. Evers, R.A. Gemeinhart, T.L. Li, Biodistribution and bioimaging studies of hybrid paclitaxel nanocrystals: lessons learned of the EPR effect and image-guided drug delivery, J. Control. Release 172 (2013) 12–21.
[13] C.P. Hollis, H.L. Weiss, B.M. Evers, R.A. Gemeinhart, T.L. Li, *In Vivo* investigation of hybrid paclitaxel nanocrystals with dual fluorescent probes for cancer theranostics, Pharm. Res. 31 (2014) 1450–1459.
[14] H. Zhang, X.Q. Wang, W.B. Dai, R.A. Gemeinhart, Q. Zhang, T.L. Li, Pharmacokinetics and treatment efficacy of camptothecin nanocrystals on lung metastasis, Mol. Pharm. 11 (2014) 226–233.
[15] Y. Chen, T.L. Li, Cellular uptake mechanism of paclitaxel nanocrystals determined by confocal imaging and kinetic measurement, AAPS J. 17 (2015) 1126–1134.
[16] F.M. Veronese, Peptide and protein PEGylation: a review of problems and solutions, Biomaterials 22 (2001) 405–417.
[17] W. Yang, L. Zhang, S. Wang, A.D. White, S. Jiang, Functionalizable and ultra stable nanoparticles coated with zwitterionic poly(carboxybetaine) in undiluted blood serum, Biomaterials 30 (2009) 5617–5621.
[18] R. Gref, Y. Minamitake, M.T. Peracchia, V. Trubetskoy, V. Torchilin, R. Langer, Biodegradable long-circulating polymeric nanospheres, Science 263 (1994) 1600–1603.
[19] H. Otsuka, Y. Nagasaki, K. Kataoka, PEGylated nanoparticles for biological and pharmaceutical applications, Adv. Drug. Deliv. Rev. 55 (2003) 403–419.
[20] J.Y. Kim, J.K. Kim, J.S. Park, Y. Byun, C.K. Kim, The use of PEGylated liposomes to prolong circulation lifetimes of tissue plasminogen activator, Biomaterials 30 (2009) 5751–5756.
[21] J.M. Harris, R.B. Chess, Effect of pegylation on pharmaceuticals, Nat. Rev. Drug. Discov. 2 (2003) 214–221.
[22] K.L. Prime, G.M. Whitesides, Self-assembled organic monolayers: model systems for studying adsorption of proteins at surfaces, Science 252 (1991) 1164–1167.
[23] L. Zhang, Z.Q. Cao, T. Bai, L. Carr, J.R. Ella-Menye, C. Irvin, B.D. Ratner, S.Y. Jiang, Zwitterionic hydrogels implanted in mice resist the foreign-body reaction, Nat. Biotechnol. 31 (2013) 553–556.
[24] N. Bertrand, J. Wu, X.Y. Xu, N. Kamaly, O.C. Farokhzad, Cancer nanotechnology: the impact of passive and active targeting in the era of modern cancer biology, Adv. Drug Deliv. Rev. 66 (2014) 2–25.
[25] T.M. Allen, A. Chonn, Large unilamellar liposomes with low uptake into the reticuloendothelial system, FEBS Lett. 223 (1987) 42–46.
[26] A.J. Keefe, S.Y. Jiang, Poly(zwitterionic)protein conjugates offer increased stability without sacrificing binding affinity or bioactivity, Nat. Chem. 4 (2011) 59–63.
[27] R.B. Weiss, R.C. Donehower, P.H. Wiernik, T. Ohnuma, R.J. Gralla, D.L. Trump, J.R. Baker, D.A. Vanecho, D.D. Vonhoff, B. Leylandjones, Hypersensitivity reactions from taxol, J. Clin. Oncol. 8 (1990) 1263–1268.
[28] J. Szebeni, Complement activation-related pseudoallergy: a new class of drug-induced acute immune toxicity, Toxicology 216 (2005) 106–121.
[29] D. Friedland, G. Gorman, J. Treat, Hypersensitivity reactions from taxol and etoposide, J. Natl. Cancer Inst. 85 (1993) 2036.
[30] A. Gessner, R. Waicz, A. Lieske, B.R. Paulke, K. Mader, R.H. Muller, Nanoparticles with decreasing surface hydrophobicities: influence on plasma protein adsorption, Int. J. Pharm. 196 (2000) 245–249.
[31] F. Danhier, O. Feron, V. Preat, To exploit the tumor microenvironment: passive and active tumor targeting of nanocarriers for anti-cancer drug delivery, J. Control. Release 148 (2010) 135–146.
[32] S.D. Li, L. Huang, Stealth nanoparticles: high density but sheddable PEG is a key for tumor targeting, J. Control. Release 145 (2010) 178–181.
[33] N. Bertrand, J.C. Leroux, The journey of a drug-carrier in the body: an anatomo-physiological perspective, J. Control. Release 161 (2012) 152–163.
[34] W. Gao, B. Xiang, T.T. Meng, F. Liu, X.R. Qi, Chemotherapeutic drug delivery to cancer cells using a combination of folate targeting and tumor microenvironment-sensitive polypeptides, Biomaterials 34 (2013) 4137–4149.
[35] T. Desmettre, J.M. Devoisselle, S. Mordon, Fluorescence properties and metabolic features of indocyanine green (ICG) as related to angiography, Surv. Ophthalmol. 45 (2000) 15–27.
[36] G. Shafirstein, W. Baumler, L.J. Hennings, E.R. Siegel, R. Friedman, M.A. Moreno, J. Webber, C. Jackson, R.J. Griffin, Indocyanine green enhanced near-infrared laser treatment of murine mammary carcinoma, Int. J. Cancer 130 (2012) 1208–1215.
[37] B. Hollins, B. Noe, J.M. Henderson, Fluorometric determination of indocyanine green in plasma, Clin. Chem. 33 (1987) 765–768.